

CHEMISTRY

A European Journal

A Journal of



Accepted Article

Title: Nitrogen and fluorine-codoped carbon nanowire aerogels as metal-free electrocatalysts for oxygen reduction reaction

Authors: Shaofang Fu, Chengzhou Zhu, Junhua Song, Mark Engelhard, Biwei Xiao, Dan Du, and Yuehe Lin

This manuscript has been accepted after peer review and appears as an Accepted Article online prior to editing, proofing, and formal publication of the final Version of Record (VoR). This work is currently citable by using the Digital Object Identifier (DOI) given below. The VoR will be published online in Early View as soon as possible and may be different to this Accepted Article as a result of editing. Readers should obtain the VoR from the journal website shown below when it is published to ensure accuracy of information. The authors are responsible for the content of this Accepted Article.

To be cited as: *Chem. Eur. J.* 10.1002/chem.201701969

Link to VoR: <http://dx.doi.org/10.1002/chem.201701969>

Supported by
ACES

WILEY-VCH

Nitrogen and fluorine-codoped carbon nanowire aerogels as metal-free electrocatalysts for oxygen reduction reaction

Shaofang Fu,^[a] Chengzhou Zhu,^{*[a]} Junhua Song,^[a] Mark H. Engelhard,^[b] Biwei Xiao,^[c] Dan Du,^[a] Yuehe Lin^{*[a]}

Abstract: The development of active, durable and low-cost catalysts to replace noble metal-based materials is highly desirable to promote the sluggish oxygen reduction reaction in fuel cells. Herein, nitrogen and fluorine-codoped three-dimensional carbon nanowire aerogels, composed of interconnected carbon nanowires were for the first time synthesized by hydrothermal carbonization process. Owing to their porous nanostructures and heteroatom-doping, the as-prepared carbon nanowire aerogels with optimized composition present excellent electrocatalytic activity that is comparable to commercial Pt/C. Remarkably, the aerogels also exhibit superior stability and methanol tolerance. This synthesis procedure paves a new way to design novel heteroatom-doped catalysts.

Introduction

Pt-based nanomaterials have been widely used as catalysts to facilitate the sluggish oxygen reduction reaction (ORR) due to their good catalytic activity and 4-electron transfer process.¹⁻³ However, the precious metals are expensive and scarce, which hinders their practical applications in industry.⁴⁻⁶ In order to reduce or even replace the precious metals, many efforts have been made in developing non-precious metal and metal-free catalysts.⁷⁻¹³ Among these noble metal-free catalysts, catalytically active carbon materials are one class of the most promising candidates. They are expected to prevent corrosion or poisoning of metal-based active sites, thus rendering superior stability. Carbon aerogels, composed of interconnected one-dimensional (1D) or two-dimensional (2D) building blocks such as carbon nanofibers/nanowires or graphene nanosheets, have attracted intensive attentions, because they not only inherit the properties of the unique building blocks, but also possess structural and electrical advantages.¹⁴⁻¹⁷ Owing to their low cost, good conductivity, large surface area, and sufficient durability

under harsh environment, these carbon aerogels are promising candidates for ORR electrocatalysts.

Aside from the morphological control, introduction of heteroatoms (B, N, P, S and F) into the carbon structure is another efficient strategy to improve the ORR activity of carbon-based electrocatalysts.¹⁸⁻²⁴ Theoretically, the electronegativity difference between heteroatoms and carbon breaks the electroneutrality of adjacent carbon atoms, thus generating charged sites, which have been demonstrated to be favorable for O₂ adsorption and charge transfer in ORR.^{4, 19}

Herein, we for the first time successfully fabricated N and F-codoped carbon nanowire aerogels (NFCNAs) through template-directed hydrothermal carbonization. By adjusting the doping level and carbonization condition, the electrocatalytic activity of the NFCNAs was tuned in a wide range. Due to the synergistic effect of dopants, good conductivity, large surface area and high porosity, the as-synthesized NFCNAs catalysts obtained under optimized condition present good ORR catalytic performance in alkaline solution that is comparable to Pt/C.

Results and Discussion

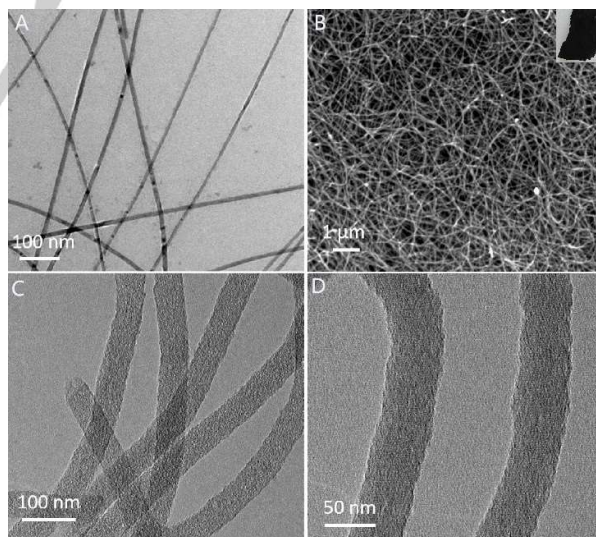


Figure 1. (A) TEM image of Te NWs. (B) SEM image of NFCNAs-18-1000 (inset: the corresponding digital picture). (C, D) TEM images of NFCNAs-18-1000.

[a] S. Fu, Dr. C. Zhu, J. Song, Dr. D. Du, Prof. Y. Lin
School of Mechanical and Materials Engineering
Washington State University, Pullman, WA 99164, USA
E-mail: chengzhou.zhu@wsu.edu; yuehe.lin@wsu.edu

[b] M. Engelhard
Environmental Molecular Sciences Laboratory
Pacific Northwest National Laboratory, Richland, WA 99352, USA

[c] Energy and Environmental Directory, Pacific Northwest National
Laboratory, Richland, WA 99352, USA

Supporting information for this article is given via a link at the end of the document.

So far, several strategies have been reported to synthesize F-doped nanomaterials, including chemical vapor deposition, arc discharge and plasma process.^{25, 26, 27} However, these methods are hard to get extensive applications because of their high cost, rigorous condition, high voltage and specific equipment requirement.²⁸ In this work, Te nanowires (NWs) were utilized as hard templates to fabricate NFCNAs because of their ultra-thin diameter, good dispersion and large-scale availability (Figure 1A).²⁹ Typically, Te NWs were first synthesized and then dispersed in glucose solution to form a uniform mixture. Further hydrothermal treatment under 180 °C for 15 h resulted in carbon hydrogels. After removal of residuals, the hydrogels were soaked in a certain amount of NH₄F solution for 12 h. The final products were obtained by freeze-drying and carbonization at 1000 °C for 1 h with a heating/cooling rate of 5 °C /min (Figure 1B inset), leading to the graphitization of NFCNAs and decomposition of Te templates. By varying the mass ratio between NH₄F and carbon materials, different aerogels were obtained and donated as NFCNAs-R-1000 (R = NH₄F/carbon materials mass ratio). The typical scanning electron microscopy (SEM) image of NFCNAs-18-1000 in Figure 1B shows that NFCNAs exhibit highly porous 3D networks, composed of interconnected carbon NWs with uniform size. It has been proposed that the formation of carbonaceous matrices was induced by dehydration and polymerization of glucose during the hydrothermal process. In the meantime, the NWs interconnected with each other and self-assembled into 3D hydrogels.^{15, 24} The detailed structure of the NWs in NFCNAs was further characterized by transmission electron microscope (TEM). The uniformly distributed NWs are clearly shown in Figure 1B with an average diameter of ~51 nm. Similar structures can also be observed in NFCNAs-9-1000 and NFCNAs-25-1000 as revealed in Figure S1. Furthermore, the effect of the pyrolysis condition on the morphology of NFCNAs was also studied. As shown in Figure S2, the typical hollow structure can be seen in NFCNAs-18-800 and NFCNAs-18-900 with an inner diameter of ~ 10 nm, which matches well with the thickness of Te NWs. The hollow structure was also observed in CAN-1000 (Figure S3). It is worth noting that the disappearance of a hollow structure in NFCNAs-9-1000, NFCNAs-18-1000 and NFCNAs-25-1000 might be attributed to the high pyrolysis temperature as well as the introduction of F and N.

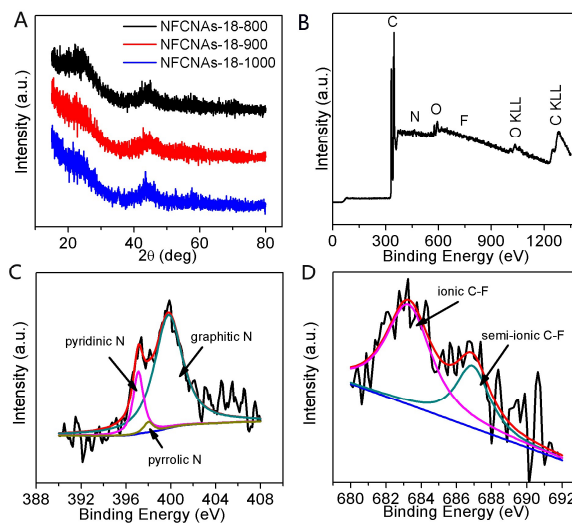


Figure 2. (A) XRD patterns of NFCNAs-18 at different annealing temperatures. XPS spectrum (B) and high resolution XPS spectra of N (C) and F (D) in NFCNAs-18-1000.

To gain insight into the crystal structure of the aerogels, X-ray diffraction (XRD) was performed as revealed in Figure 2A. The XRD patterns show the existence of two characteristic peaks at ~24.7° and 44.1°, corresponding to (002) and (100) plane of graphitic carbon, regardless of the pyrolysis temperature.^{30, 31} In order to investigate the surface composition of NFCNAs, X-ray photoelectron spectroscopy (XPS) analysis was conducted, as shown in Figure 2B-D. The XPS quantitative results show that the atomic ratio of C, O, N and F in NFCNAs-18-1000 is 93.96%, 4.2%, 1.8% and 0.04%, respectively. The N 1s spectrum of NFCNAs-18-1000 was further deconvoluted into three functional groups (Figure 2C), which include pyridinic-N (397.1 eV), pyrrolic-N (398.1 eV), and graphitic-N (400.0 eV). The deconvolution results reveal that more atoms are in the form of pyridinic N and graphitic-N, which favors the ORR catalytic activity.^{32, 33} Two peaks can be observed in F 1s XPS spectrum in Figure 2D, that are corresponding to ionic C-F bond (683.3 eV) and semi-ionic C-F bond (686.9 eV). It has been demonstrated in the reported works that the F^{δ-} in the ionic and semi-ionic C-F bonds is different from free F ions in the solution.³⁴ In NFCNAs, F^{δ-} still bonds tightly with C^{δ+} and shows some ionic characters. The higher ratio of ionic C-F bond (69%) can also contribute to the good ORR catalytic activity of the NFCNAs. In addition, N₂ adsorption/desorption measurement was carried to analyze the surface area and pore size distribution of NFCNAs-18-1000. The Brunauer-Emmett-Teller surface area and pore volume are 768.4 m²/g and 0.5 cm³/g (Figure S4), respectively. The pore size distribution profile indicates that mesopores are dominant in NFCNAs-18-1000. This novel porous structure with large surface area contributes to faster mass transport and electron transfer process, leading to enhanced catalytic performance.

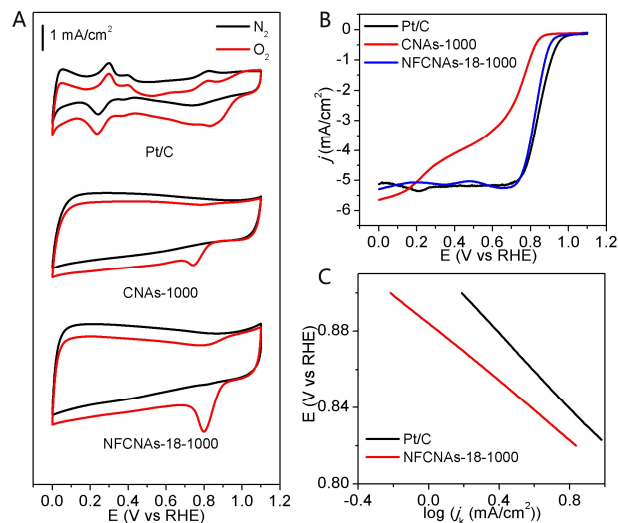


Figure 3. (A) CV curves of Pt/C, CNAs-1000, and NFCNAs-18-1000 in N₂ and O₂-saturated 0.1 M KOH solution with a scan rate of 50 mV/s. (B) LSV curves of catalysts with a scan rate of 10 mV/s at a rotating rate of 1600 rpm. (C) Tafel plots of commercial Pt/C and NFCNAs-18-1000 catalysts.

The electrocatalytic activities of the as-synthesized aerogels were evaluated and compared with commercial Pt/C catalyst by cyclic voltammetry (CV) measurements in N₂ and O₂-saturated 0.1 M KOH solution with a scan rate of 50 mV/s. Figure 3A reveals that all the catalysts display well-defined cathodic peaks in O₂-saturated electrolyte while no peak is found in N₂-saturated solution. Remarkably, NFCNAs-18-1000 presents a more positive peak potential compared with that of the undoped aerogels (CNAs-1000). This value is even comparable with that observed on Pt/C catalyst, indicating the enhanced ORR electrocatalytic activity of NFCNAs-18-1000. To further demonstrate the good catalytic activity of the NFCNAs, we performed linear sweep voltammetry (LSV) using rotating disk electrode (RDE) in O₂-saturated 0.1 M KOH solution. Figure 3B reveals the LSV curves for CNAs-1000, NFCNAs-18-1000, and commercial Pt/C catalysts with a rotating rate of 1600 rpm and a scan rate of 10 mV/s. Compared with CNAs-1000 (0.841 and 0.697 V), NFCNAs-18-1000 shows a more positive onset potential and half-wave potential of 0.912 and 0.825 V, which are comparable to that of Pt/C (0.934 and 0.844 V). To investigate the intrinsic advantages of the unique structure, the Tafel plots are derived from the LSV curves of these three samples and shown in Figure 3C. The Tafel slope for NFCNAs-18-1000 is about 70 mV/dec, which is smaller than that of commercial Pt/C (99 mV/dec), demonstrating a faster kinetic process of ORR on NFCNAs-18-1000 electrode. It is worth noting that the catalytic activity of NFCNAs-18-1000 is comparable with or even outperforms some reported catalysts (Table S1). Moreover, the ORR catalytic activity of the aerogels with different composition was also investigated. Figure S5B presents that NFCNAs-18-1000 has a more positive onset potential and half-wave potential than that of NFCNAs-9-1000

and NFCNAs-25-1000, which mainly attributes to the larger electrochemical surface area (Figure S5A) and rational N and F content. Figure S6 displays the effect of the pyrolysis condition on the ORR activity of the aerogels. We can see much better catalytic performance on NFCNAs-18-1000 electrode due to the high electrochemical surface area (Figure S6A) as well as the synergistic effect of dopants with proper composition of heteroatoms.

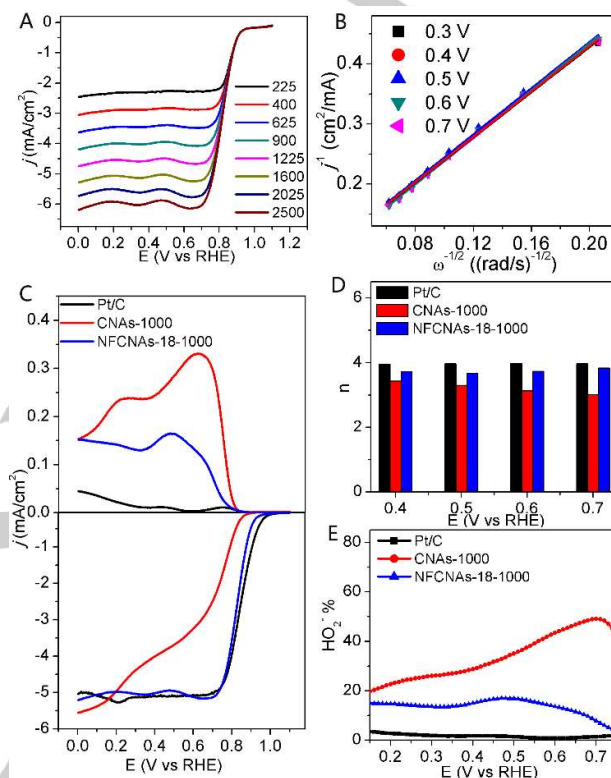


Figure 4. (A) LSV curves of NFCNAs-18-1000 in O₂-saturated 0.1 M KOH solution under different rotating rate. (B) The corresponding K-L plots at different voltages. (C) LSV curves of catalysts recorded using RRDE with a scan rate of 10 mV/s at a rotating rate of 1600 rpm. (D) Number of transferred electrons on Pt/C, CNAs-1000, and NFCNAs-18-1000. (E) H₂O₂ yield on different catalysts based on RRDE data.

To study the ORR process on the catalysts, the Koutecky-Levich (K-L) plots were obtained at different potential based on the LSV curves with various rotating speeds (Figure 4A). The good linearity and parallelism in Figure 4B suggests the first-order reaction kinetics regarding the dissolved oxygen in the solution.^{35, 36} It is generally accepted that ORR is a multi-step process via either a direct four-electron pathway or a two-electron pathway with HO₂⁻ as the intermediate species. A four-electron pathway is highly desired for the catalyst since this can obtain better ORR efficiency.⁵ The number of electron transferred (n) on different electrodes were calculated from the ring and disk currents obtained from the rotation ring-disk electrode (RRDE) measurements (Figure 4C) based on equation

1.³⁷ The average n value for NFCNAs-18-1000 is 3.7, which is similar as Pt/C ($n=3.97$), as shown in Figure 4D. According to the RRDE results, the HO_2^- yield were also obtained from equation 2.^{37, 38} Figure 4E shows the HO_2^- produced on different catalysts. In comparison with CNAs-1000, which presents a high HO_2^- value, NFCNAs-18-1000 yields much lower HO_2^- over a large potential range, further confirming its higher ORR efficiency.

$$n = 4 \times \frac{I_D}{I_D + I_R/N} \quad (1)$$

$$\text{HO}_2^- \% = 200 \frac{I_R/N}{I_D + I_R/N} \quad (2)$$

where I_D and I_R is the disk and ring current, respectively, which can be obtained according to Figure 4C. $N=0.37$ is the collection efficient.

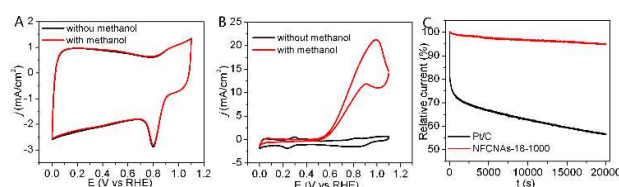


Figure 5. CV curves of NFCNAs-18-1000 (A) and Pt/C (B) with and without the addition of 1 M methanol. (C) Current vs time curves obtained under 0.7 V for Pt/C and NFCNAs-18-1000 in O₂-saturated 0.1 M KOH at a rotating rate of 200 rpm.

To further demonstrate the superior catalytic performance of NFCNAs-18-1000, its tolerance to methanol and durability were also studied. Small molecules, such as methanol, can transport through the membrane easily, thus reducing the cathodic reactant. Moreover, the intermediate product (e.g. carbon monoxide) might adsorb onto the surface of the catalysts, leading to the poisoning of the cathode materials. All these effects can lower the efficiency of the fuel cells. Both NFCNAs-18-1000 and commercial Pt/C catalysts were subjected to the methanol crossover tests to evaluate their tolerance to methanol. NFCNAs-18-1000 presents a stable CV curve without any electroactivity specific to methanol when it was added into the solution (Figure 5A), demonstrating the remarkable tolerance to methanol crossover effect of the NFCNAs-18-1000 electrode. In contrast, Pt/C shows a characteristic methanol oxidation/reduction peaks with the addition of 1 M methanol (Figure 5B). Figure 5C displays the relative current vs time curves obtained under 0.3 V for Pt/C and NFCNAs-18-1000 in O₂-saturated 0.1 M KOH at a rotating rate of 200 rpm, where NFCNAs-18-1000 only lost 5% of its original activity over 20000 s of the continuous reaction. However, a substantial loss of current (44%) is observed on the commercial Pt/C. The superiority of the stability on NFCNAs-18-1000 electrode was also demonstrated by its morphology change. No obvious changes can be observed in the TEM images of NFCNAs-18-1000 after the stability test, while the Pt/C catalyst shows a severe aggregation of the Pt particles (Figure S7). The superior

stability of NFCNAs-18-1000 is mainly attributed to the following factors: 1) the unique porous 3D structure composed of interconnected NWs is expected to provide large surface area, fast electron-transfer as well as remarkable structural robustness in alkaline condition; 2) The more electronegativity of N and F induces positive charges on nearby C atoms, which can not only provide faster charge-transfer but promote O₂ to adsorb on the surface of catalysts. By virtue of the synergistic effect between N and F as well as the proper doping level, the as-prepared NFCNAs exhibit enhanced catalytic activity for ORR. 3) In contrast to the free F ions in the solution, F⁻ in the ionic and semi-ionic C-F tightly bonds with C^{δ+}, making the catalysts less vulnerable to corrosion, resulting in better stability.

Conclusions

In this work, we demonstrated a facile strategy to synthesize the N, F-codoped metal-free ORR catalysts by combining the hard-templating method and hydrothermal carbonization. By tuning the concentration of dopant and the pyrolysis condition, we successfully fabricated a class of NFCNAs, which are composed of interconnected carbon nanowires with the diameter ~ 50 nm. This synthesis procedure achieves simultaneous optimization of both surface functionality and 3D porous structure, leading to the comparable ORR activity to that of commercial Pt/C in alkaline solution. Importantly, the NFCNAs synthesized under optimized condition exhibit excellent long-term stability and good tolerance to methanol crossover effect. This superior electrocatalytic performance should be attributed to the synergistic effect of dopants with optimal composition, highly porous structure, and the unique 3D interconnected morphology, which could not only facilitate the mass-transport and electron-transfer during ORR process but eliminate the aggregation and dissolution effects existing in metal nanoparticles-based catalysts.³⁹ This synthetic protocol for the development of N, F-codoped carbon nanowire aerogels might show potential applications in the development of other metal-free electrocatalysts with enhanced ORR performance.

Experimental Section

Experimental section is available in supporting information.

Acknowledgements

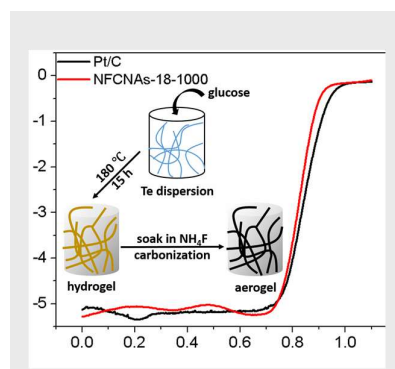
This work was supported by a start-up fund of Washington State University, USA. The XPS analysis was performed using EMSL, a national scientific user facility sponsored by the Department of Energy's Office of Biological and Environmental Research and located at Pacific Northwest National Laboratory (PNNL). We acknowledge Franceschi Microscopy & Image Center at Washington State University for TEM measurements. PNNL is a multi-program national laboratory operated for DOE by Battelle under Contract DE-AC05-76RL01830.

Keywords: porous nanostructures • heteroatom-doped nanomaterials • carbon aerogels • metal-free catalysts • oxygen reduction reaction

- [1] Alia, S. M.; Jensen, K.; Contreras, C.; Garzon, F.; Pivovar, B.; Yan, Y. S. *ACS Catal.* **2013**, *3*, 358-362.
- [2] Ma, L.; Wang, C. M.; Xia, B. Y.; Mao, K. K.; He, J. W.; Wu, X. J.; Xiong, Y. J.; Lou, X. W. *Angew. Chem. Int. Ed.* **2015**, *54*, 5666-5671.
- [3] Xia, B. Y.; Yan, Y.; Li, N.; Wu, H. B.; Lou, X. W.; Wang, X. *Nat. Energy* **2016**, *1*, 15006.
- [4] Wei, W.; Tao, Y.; Lv, W.; Su, F. Y.; Ke, L.; Li, J.; Wang, D. W.; Li, B. H.; Kang, F. Y.; Yang, Q. H. *Sci. Rep.* **2014**, *4*, 6289.
- [5] Zhu, C. Z.; Li, H.; Fu, S. F.; Du, D.; Lin, Y. H. *Chem. Soc. Rev.* **2016**, *45*, 517-531.
- [6] Hu, C. G.; Dai, L. M. *Angew. Chem. Int. Ed.* **2016**, *55*, 2-25.
- [7] Guan, B. Y.; Yu, L.; Lou, X. W. *Adv. Mater.* **2016**, *28*, 9596.
- [8] Hu, H.; Han, L.; Yu, M. Z.; Wang, Z. Y.; Lou, X. W. *Energ. Environ. Sci.* **2016**, *9*, 107-111.
- [9] Yang, F.; Abadia, M.; Chen, C. Q.; Wang, W. K.; Li, L.; Zhang, L. B.; Rogero, C.; Chuvillin, A.; Knez, M. *Nano Res.* **2017**, *10*, 97-107.
- [10] Tang, J.; Liu, J.; Torad, N. L.; Kimura, T.; Yamauchi, Y. *Nano Today* **2014**, *9*, 305-323.
- [11] Zakaria, M. B.; Malgras, V.; Takei, T.; Li, C. L.; Yamauchi, Y. *Chem. Commun.* **2015**, *51*, 16409-16412.
- [12] Yang, W. X.; Liu, X. J.; Yue, X. Y.; Jia, J. B.; Guo, S. J. *J. Am. Chem. Soc.* **2015**, *137*, 1436-1439.
- [13] Zhou, M.; Wang, H. L.; Guo, S. J. *Chem. Soc. Rev.* **2016**, *45*, 1273-1307.
- [14] Fu, X. G.; Choi, J. Y.; Zamani, P.; Jiang, G. P.; Hoque, M. A.; Hassan, F. M.; Chen, Z. W. *ACS Appl. Mater. Inter.* **2016**, *8*, 6488-6495.
- [15] Liang, H. W.; Guan, Q. F.; Chen, L. F.; Zhu, Z.; Zhang, W. J.; Yu, S. H. *Angew. Chem. Int. Ed.* **2012**, *51*, 5101-5105.
- [16] Wu, Z. Y.; Li, C.; Liang, H. W.; Chen, J. F.; Yu, S. H. *Angew. Chem. Int. Ed.* **2013**, *52*, 2925-2929.
- [17] Xu, C. C.; Su, Y.; Liu, D. J.; He, X. Q. *Phys. Chem. Chem. Phys.* **2015**, *17*, 25440-25448.
- [18] Zhang, C. Z.; Mahmood, N.; Yin, H.; Liu, F.; Hou, Y. L. *Adv. Mater.* **2013**, *25*, 4932-4937.
- [19] Guan, B. Y.; Yu, L.; Lou, X. W. *J. Am. Chem. Soc.* **2016**, *138*, 11306.
- [20] You, C. H.; Zen, X. Y.; Qiao, X. C.; Liu, F. F.; Shu, T.; Du, L.; Zeng, J. H.; Liao, S. J. *Nanoscale* **2015**, *7*, 3780-3785.
- [21] Tahir, M.; Mahmood, N.; Zhu, J. H.; Mahmood, A.; Butt, F. K.; Rizwan, S.; Aslam, I.; Tanveer, M.; Idrees, F.; Shakir, I.; Cao, C. B.; Hou, Y. L. *Sci. Rep.* **2015**, *5*, 12389.
- [22] Yang, D. S.; Bhattacharjya, D.; Inamdar, S.; Park, J.; Yu, J. S. *J. Am. Chem. Soc.* **2012**, *134*, 16127-16130.
- [23] Zhang, C.; An, B.; Yang, L.; Wu, B. B.; Shi, W.; Wang, Y. C.; Long, L. S.; Wang, C.; Lin, W. B. *J. Mater. Chem. A* **2016**, *4*, 4457-4463.
- [24] Zhu, C. Z.; Fu, S. F.; Song, J. H.; Shi, Q. R.; Su, D.; Engelhard, M. H.; Li, X. L.; Xiao, D. D.; Li, D. S.; Estevez, L.; Du, D.; Lin, Y. H. *Small* **2017**, *13*, 1603407.
- [25] Liu, L. S.; Mei, Z. X.; Hou, Y. N.; Liang, H. L.; Azarov, A.; Venkatachalapathy, V.; Kuznetsov, A.; Du, X. L. *Sci. Rep.* **2015**, *5*, 15516.
- [26] Carraro, G.; Gasparotto, A.; Maccato, C.; Bontempi, E.; Lebedev, O. I.; Turner, S.; Sada, C.; Depero, L. E.; Tendeloo, G. V.; Barreca, D. *RSC Adv.* **2013**, *3*, 23762-23768.
- [27] Miinea, L. A.; Hoffman, D. M. *J. Mater. Chem.* **2000**, *10*, 2392-2395.
- [28] Huang, S. Z.; Li, Y.; Feng, Y. Y.; An, H. R.; Long, P.; Qin, C. Q.; Feng, W. *J. Mater. Chem. A* **2015**, *3*, 23095-23105.
- [29] Hong, W.; Wang, J.; Wang, E. K. *Nano Res.* **2015**, *8*, 2308-2316.
- [30] Xu, T.; Zhang, H. M.; Zhong, H. X.; Ma, Y. W.; Jin, H.; Zhang, Y. N. *J. Power Sources* **2010**, *195*, 8075-8079.
- [31] Liang, J.; Zhou, R. F.; Chen, X. M.; Tang, Y. H.; Qiao, S. Z. *Adv. Mater.* **2014**, *26*, 6074-6079.
- [32] Choi, C. H.; Chung, M. W.; Kwon, H. C.; Chung, J. H.; Woo, S. I. *Appl. Catal. B-Environ.* **2014**, *144*, 760-766.
- [33] Guo, D. H.; Shibuya, R.; Akiba, C.; Saji, S.; Kondo, T.; Nakamura, J. *Science* **2016**, *351*, 361-365.
- [34] Sun, X. J.; Song, P.; Zhang, Y. W.; Liu, C. P.; Xu, W. L.; Xing, W. *Sci. Rep.* **2013**, *3*, 2505.
- [35] Mayrhofer, K. J. J.; Strmcnik, D.; Blizanac, B. B.; Stamenkovic, V.; Arenz, M.; Markovic, N. M. *Electrochim. Acta* **2008**, *53*, 3181-3188.
- [36] Fu, S. F.; Zhu, C. Z.; Zhou, Y. Z.; Yang, G. H.; Jeon, J. W.; Lemmon, J.; Du, D.; Nune, S. K.; Lin, Y. H. *Electrochim. Acta* **2015**, *178*, 287-293.
- [37] Liang, Y. Y.; Wang, H. L.; Zhou, J. G.; Li, Y. G.; Wang, J.; Regier, T.; Dai, H. J. *J. Am. Chem. Soc.* **2012**, *134*, 3517-3523.
- [38] Zhai, Y. L.; Zhu, C. Z.; Wang, E. K.; Dong, S. J. *Nanoscale* **2014**, *6*, 2964-2970.
- [39] Sun, S. H.; Zhang, G. X.; Geng, D. S.; Chen, Y. G.; Li, R. Y.; Cai, M.; Sun, X. L. *Angew. Chem. Int. Ed.* **2011**, *50*, 422-426.

FULL PAPER

N, F-codoped carbon nanowire aerogels were synthesized by hydrothermal carbonization procedure. The functionalized aerogels present high electrocatalytic activity, superior stability and methanol-tolerance for ORR in alkaline condition.



Shaofang Fu, Chengzhou Zhu,* Junhua Song, Mark H. Engelhard, Biwei Xiao, Dan Du, Yuehe Lin*

Page No. – Page No.

Nitrogen and fluorine-codoped carbon nanowire aerogels as metal-free electrocatalysts for oxygen reduction reaction